Chemistry–A European Journal
Research Article
doi.org/10.1002/chem.202302129
Chemistry Europe
European Chemical Societies Publishing
www.chemeurj.org

Special Collection

Photoreduction of Anthracenes Catalyzed by *peri*-Xanthenoxanthene: a Scalable and Sustainable Birch-Type Alternative

Cristian De Luca[+],[a] Davide Zanetti[+],[a] Tommaso Battisti,[b] Rúben R. Ferreira,[a] Sofia Lopez,[c] Alexander H. McMillan,[d] Sasha Cai Lesher-Pérez,[e] Laura Maggini,[a] and Davide Bonifazi*[a]

Dedicated to Prof. Dr. Maurizio Prato on the occasion of his 70th birthday.

The typical Birch reduction transforms arenes into cyclohexa-1,4-dienes by using alkali metals, an alcohol as a proton source, and an amine as solvent. Capitalizing on the strong photoreductive properties of *peri*-xanthenoxanthene (PXX), herein we report the photocatalyzed "Birch-type" reduction of acenes by employing visible blue light irradiation at room temperature in the presence of air. Upon excitation at 405 or 460 nm in the presence of a mixture of *N*,*N*-diisopropylethylamine (DIPEA) and trifluoromethanesulfonimide ($HNTf_2$) in DMSO, PXX photocatalyzes the selective reduction of full-carbon acene derivatives (24–75%). Immobilization of PXX onto polydimethylsiloxane (PDMS) beads (PXX-PDMS) allowed the use of the catalyst in heterogeneous batch reactions, giving 9-phenyl-9,10-dihydroanthracene in high yield (68%). The catalyst could easily be recovered and reused, with no notable drop in performance observed after five reaction cycles. Integration of the PXX-PDMS beads into a microreactor enabled the reduction of acenes under continuous-flow conditions, thereby validating the sustainability and scalability of this heterogeneous-phase approach.

Introduction

The classical Birch reduction, first reported by Arthur Birch in 1944,[1–3] involves the perilous condensation of NH_3 at cryogenic temperatures in the presence of pyrophoric metals to produce solvated electrons capable of performing the reduction of unactivated arenes ($E_{red} < -3.42$ V vs SCE).[4] The regioselectivity of the protonation depends on the nature of the substituents on the aromatic ring, with electron-donating and electron-withdrawing groups favoring *ortho* and *para* protonation, respectively. This reaction allows the introduction of saturation and functional groups into aromatic compounds. However, the applicability of the classical Birch reduction has been limited due to safety, environmental, and technical concerns, and difficulty in its scale-up.[5] In this context, researchers have been recently pursuing sustainable alternatives to the classical Birch reduction protocols, including NH_3-free variant,[6–9] electrochemical,[5,10,11] and mechanochemical approaches.[12,13]

Recently, catalysts displaying strong reductive photoredox properties ($E_{red} < -2.00$ V vs SCE)[14–18] have emerged as alternative tools to trigger reduction reactions and generate radical anions under mild reaction conditions.[19–22] The first photocatalyzed variant of the Birch reduction of arene-type derivatives (e.g., naphthalenes, acene-type aromatic hydrocarbons, and heterocycles; Scheme 1) was reported by Chatterjee and König.[19] The authors proposed that upon visible-light photoexcitation, the lowest triplet excited state of an Ir^{III}-based photocatalyst sensitizes the formation of a triplet state of the aromatic substrate. The latter undergoes reductive single electron transfer (SET) yielding a radical anion intermediate that, through hydrogen-atom transfer (HAT) and protonation reaction, leads to the final dearomatized product. In pursuit of a

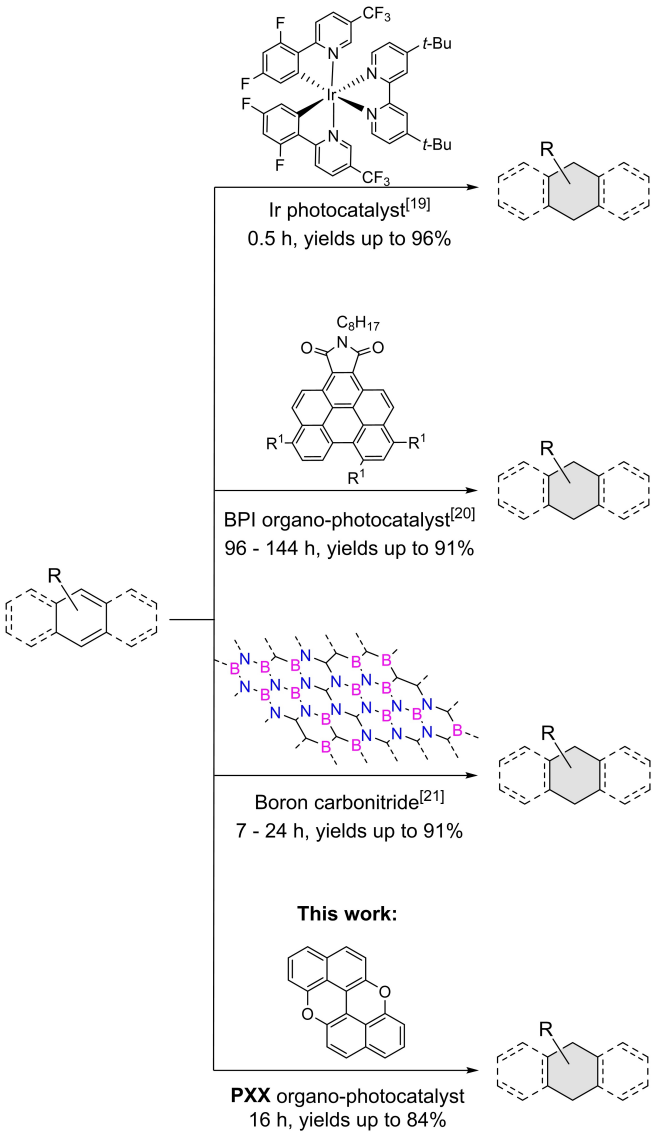
[a] C. De Luca,[+] D. Zanetti,[+] R. R. Ferreira, Dr. L. Maggini, Prof. Dr. D. Bonifazi
Institute of Organic Chemistry, University of Vienna
Währinger Strasse 38, 1090 Vienna (Austria)
E-mail: davide.bonifazi@univie.ac.at
[b] Dr. T. Battisti
School of Chemistry, Cardiff University
Park Place CF10 3AT, Cardiff (UK)
[c] S. Lopez
División Polímeros Nanoestructurados
Instituto de Investigaciones en Ciencia y Tecnología de Materiales (INTEMA)
UNMdP–CONICET y Departamento de Química, UNMdP
Av. Cristóbal Colón 10850, Mar del Plata,
B7606BWV Buenos Aires (Argentina)
[d] Dr. A. H. McMillan
Elvesys Microfluidics Innovation Center
75011 Paris (France)
[e] Dr. S. C. Lesher-Pérez
Department of Chemical Engineering
Department of Biomedical Engineering
University of Michigan
North Campus Research Complex Building 28, 2800 Plymouth Rd,
48109-2800 Ann Arbor, MI (USA)
[+] These authors contributed equally to this manuscript.

Supporting information for this article is available on the WWW under https://doi.org/10.1002/chem.202302129

Special Collection This article is part of a joint Special Collection in honor of Maurizio Prato.

© 2023 The Authors. Chemistry - A European Journal published by Wiley-VCH GmbH. This is an open access article under the terms of the Creative Commons Attribution Non-Commercial License, which permits use, distribution and reproduction in any medium, provided the original work is properly cited and is not used for commercial purposes.

© 2023 The Authors. Chemistry - A European Journal published by Wiley-VCH GmbH



Scheme 1. Photocatalyzed Birch-type reduction of anthracene-based substrates.

visible-light photocatalyzed Birch reaction targeting the reduction of benzene and its derivatives, Miyake's research group developed a benzo[*ghi*]perylene imide-based photoredox catalyst.[20] The catalyst allowed the direct reduction of benzene and its derivatives under mild benchtop conditions and visible-light (405 nm) LED irradiation under N_2. In another research avenue, Wang and co-workers prepared a boron carbonitride (BCN) semiconductor for the photo-induced hydrogenation of arenes and heteroarenes (yields up to 91%) in water with the addition of sodium dodecyl sulfate (SDS).[21] The heterogeneous transformation takes place under blue light irradiation (450 nm) and inert atmosphere following a two-photon reaction mechanism. In a recent paper, Chiba and coworkers described the use of polysulfide anions as a potent photoreducer, promoting photoinduced dearomatization of naphthalene substrates bearing acyloxy and acylamino groups under visible light irradiation.[22] Following a radical-polar crossover mechanism induced by SET from photoexcited polysulfide anions, the authors could dearomatize naphthalenes, indoles, and associated heteroaromatic derivatives.

Aiming to design, program, and prepare functional chromophores that, among other applications, could be used as strong reductive photocatalysts, our group first purposed the simple and inexpensive dye *peri*-xanthenoxanthene (PXX) to trigger photoredox transformations.[23–27] Structural simplicity, ease, and low-cost synthesis (see the Supporting Information), stability towards air and water, and good solubility in common organic solvents crowned this chromophore for application in photocatalysis.[22,23] Upon irradiation with blue light (405 or 460 nm), PXX can access its singlet excited state (^{1}PXX*). The latter is characterized by a remarkable reduction potential ($E_{1/2}^{PXX^{\bullet+}/PXX^*} = -2.00$ V vs SCE), ranking it among the strongest organic single electron transfer (SET) reductive photocatalysts reported so far.[23,25] We have first demonstrated that PXX can efficiently generate organic radicals via dehalogenation of electron-poor aryl and alkyl halides, later undergoing C–C bond formation with electron-rich radical traps.[24] Photoinduced arylation of cyclic ketones as well as C–S and C–N cross-coupling reactions of aryl halides with amines and thiols have been also investigated using a Ni co-catalyst.[24] Recently, the groups of Dilman and Liao expanded the use of PXX as a photocatalyst. Whereas the former group used PXX to promote iododifluoromethylation of alkenes,[28] the latter photocatalyzed the polymerization of olefins[29] and different types of fluorosulfonylation reactions.[30–33] Interestingly, both the organocatalytic atom transfer radical polymerization (O-ATRP) and the radical fluorosulfonylation of ketone-derived vinyl acetates could be performed under sunlight.

Building on these findings, in this paper we explore the use of PXX to trigger the photoreduction of acenes in Birch-type reactions under irradiation and homogeneous conditions. Furthermore, we have investigated its activity as a heterogeneous catalyst,[34,35] that is, upon grafting onto polydimethylsiloxane (PDMS) microparticles,[36] both in batch (i.e., as a floating heterogeneous catalyst) and within a flow microreactor (i.e., as a packed heterogeneous catalyst).[37–40] This strategy was specifically investigated to respond to the urge of producing truly scalable organic photocatalytic systems, accompanied by reduced environmental impact and costs associated with the possibility of facilitated separation and extended use (i.e., through recovery or continuous use).

Results and Discussion

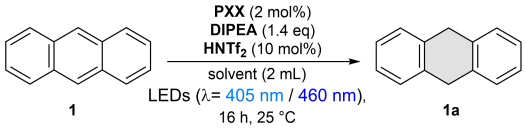
PXX as homogenous reductive photocatalyst

Our investigations started with the study of the PXX-catalyzed photoreduction of anthracene (**1**), chosen as a model aromatic substrate for its accessible reduction potential ($E_{1/2}^{Ant/Ant^{\bullet-}} > -2.00$ V vs SCE), but also for its low aromatic stabilization energy.[19] With a compatible oxidation potential of +0.52 V vs SCE, *N,N*-diisopropylethylamine (DIPEA) was chosen

© 2023 The Authors. Chemistry - A European Journal published by Wiley-VCH GmbH

as a sacrificial reductive agent to restore the catalyst as well as a source of H atoms.[23,24] The investigations started from the set of conditions previously optimized by our group for the dehalogenation of aryl compounds (2 mol% PXX, 1.4 equiv. DIPEA, DMSO, under inert atmosphere, irradiated at 405 nm).[24] Under the aforementioned conditions, PXX was able to dearomatize anthracene **1** to 9,10-dihydroanthracene **1a** with 11% yield (Table 1, entry 1). Inspired by Chatterjee's and König's protocol,[19] the addition of 10 mol% of $MeNH_3Cl$ to the reaction mixture caused a slight increase in the reduction yield (entry 2). However, moving from $MeNH_3Cl$ to trifluoromethanesulfonimide ($HNTf_2$) caused a dramatic enhancement of the reaction yield by up to 75% (entry 3). Surprisingly, the reaction was not affected by the presence of O_2 (entry 4), affording the dearomatized product in 74% yield, comparable to the yield obtained under inert atmosphere. The reaction exhibited a strong concentration dependency, with the yield dropping to 26% when halved the molarity of the solution (entry 5) and only a moderate effect of the temperature (entries 6 and 7). The loading of photocatalyst (1–10 mol%, entries 23 and 24) and $HNTf_2$ (0–100 mol%, Table S1 in the Supporting Information) were screened, confirming the optimal PXX concentration at 2 mol% (PXX aggregation is observed at higher loading)[41] and 10 mol% for $HNTf_2$. A progressive increase of the yield was observed when solvents with high polarity (CH_3CN and DMF vs toluene, CH_2Cl_2, $CHCl_3$, and THF) were used (entries 11–22), suggesting the formation of a solvent-stabilized polar intermediate (see mechanistic discussion below). Finally, control experiments were performed in the absence of either PXX, light irradiation, or DIPEA, with no dearomatized products being observed (Table 1, entries 8–10). However, in the absence of PXX (entry 8), the anthracene dimer, obtained through photo-induced [4+4] cyclization, is formed.[42,43] By changing the irradiation wavelength to 460 nm, in the presence and the absence of PXX, no dimer formation was observed, with the dearomatized product obtained in 37% yield under the former conditions (entry 25).

Table 1. General optimization of the experimental conditions for the photoreduction of anthracene into 9,10-dihydroanthracene.[a]



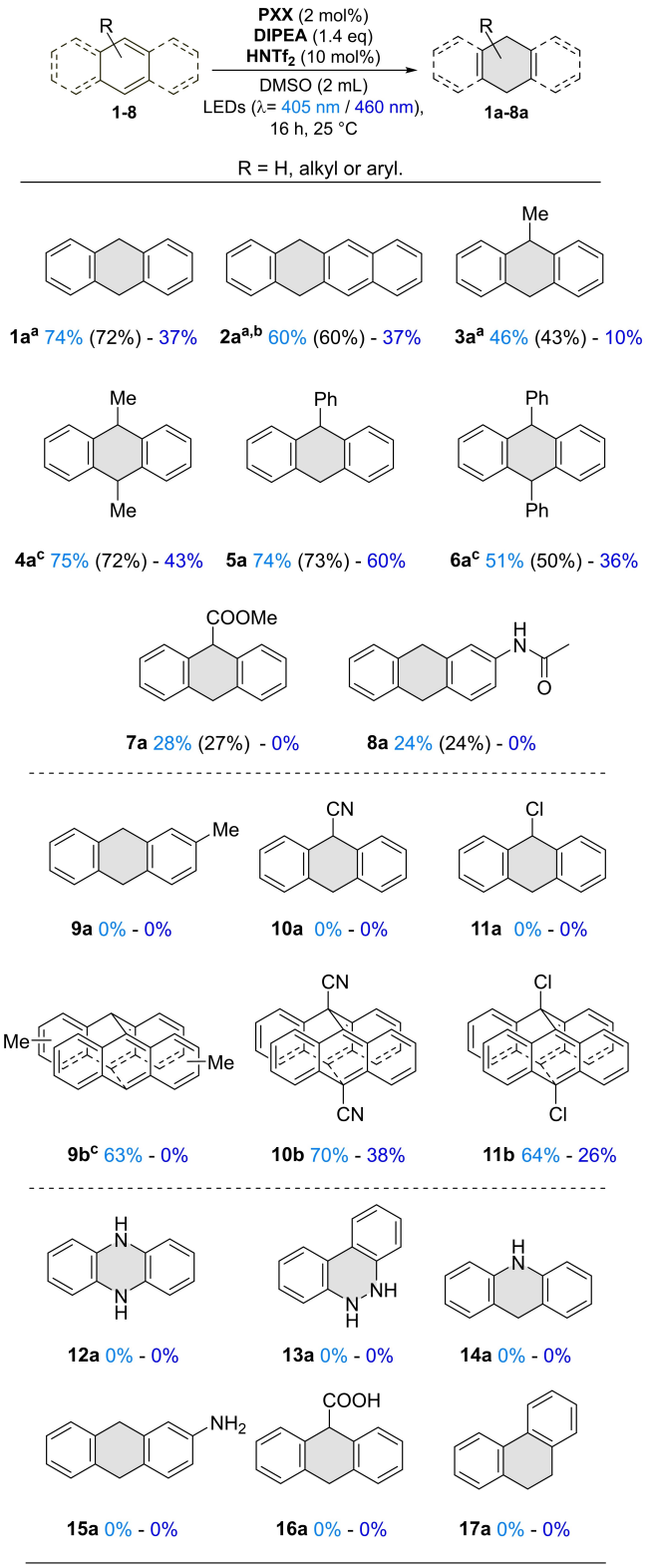
	Atmosphere	Solvent	Yield [%][b]
1[c]	Ar	DMSO	11
2[d]	Ar	DMSO	29
3	Ar	DMSO	75
4	air	DMSO	74
5	air	DMSO (4 mL)	26
6	Ar	DMSO (40 °C)	84
7	air	DMSO (40 °C)	80
8[e]	air	DMSO	–
9[f]	air	DMSO	–
10[g]	air	DMSO	–
11	Ar	benzene	<5
12	air	benzene	<5
13	Ar	THF	7
14	air	THF	6
15	Ar	CH_2Cl_2	7
16	air	CH_2Cl_2	11
17	Ar	$CHCl_3$	–
18	air	$CHCl_3$	<5
19	Ar	CH_3CN	27
20	air	CH_3CN	8
21	Ar	DMF	58
22	air	DMF	19
23[h]	air	DMSO	39
24[i]	air	DMSO	49
25[j]	air	DMSO	37

[a] The reaction was performed using (0.5 mmol) of **1**, PXX (2 mol%), DIPEA (0.7 mmol) and 2 mL of solvent. [b] Yields determined by ^1H NMR analysis using 1,3,5-trimethoxybenzene as internal standard. [c] Reaction performed without $HNTf_2$. [d] $MeNH_3Cl$ was used as proton source. [e] Reaction performed without PXX. [f] Reaction performed in the dark. [g] Reaction performed without DIPEA. [h] Reaction performed with PXX (1 mol%). [i] Reaction performed with PXX (10 mol%). [j] Reaction performed under 460 nm light irradiation.

Having the optimized reaction conditions in hand, our attention then focused on examining the generality of the PXX-triggered photo-dearomatization, by varying the framework of the polycyclic substrates (Scheme 2). Whereas our photocatalyst could not reduce benzene or naphthalene, PXX can efficiently photocatalyze the reduction of acene-type structures. A small library of anthracene derivatives with either extended conjugation (**2a**) or substituents in positions 2, 9, and 10 were reduced from moderate (24%) to good yields (75%).

Every reaction was performed with irradiation at both 405 and 460 nm (see Figure S1 for LEDs emission spectra), with the best yields obtained at 405 nm. The limited absorption of the catalyst at 460 nm significantly constrains the photocatalytic efficiency, resulting in the formation of products with reduced yields. Surprisingly, we could not perform the reduction of 2-methyl anthracene (**9**) neither exciting at 405 nor at 460 nm, and only its dimeric adducts could be observed at 405 nm in the reaction mixture. Since electrochemical studies revealed similar reduction potentials for both 9-methyl and 2-methyl anthracenes ($E_{1/2}^{M/M^{\bullet-}}$ ca. −2 V vs SCE), we could not find any plausible explanation, which does not resemble pure speculation for the unsuccessful transformation of **9** into **9a**. In the case of 9-cyano-anthracene (**10**) and 9-chloro-anthracene (**11**), no de-aromatized products could be observed in the presence of PXX, and only the dimeric products were formed under both 405 and 460 nm irradiation conditions (Scheme 2). Notably, both 9-chloro- and 9-cyano-anthracenes absorb throughout the spectral blue window till 460 nm, suggesting that the kinetics of the dimerization is faster than the photoreduction also under this irradiation. To our bewilderment, when the N-containing acenes phenazine (**12**), benzo[*c*]cinnoline (**13**), and acridine (**14**) were subjected to the reaction conditions, no conversion could

© 2023 The Authors. Chemistry - A European Journal published by Wiley-VCH GmbH



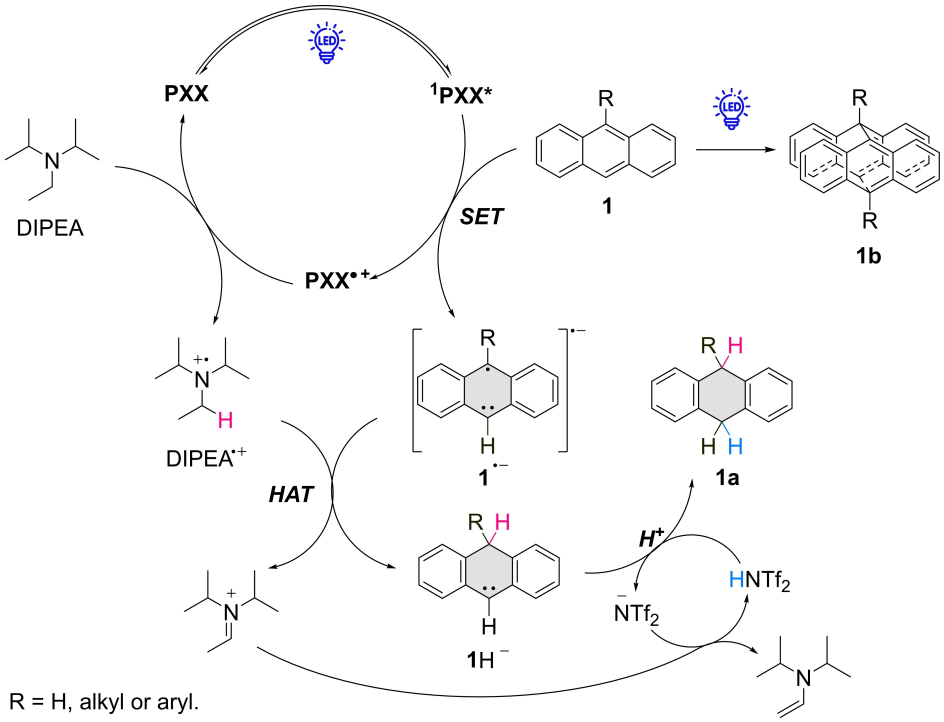
Scheme 2. Photoinduced de-aromatization reactions triggered by PXX. Reactions performed under the conditions displayed in the scheme with 0.5 mmol of anthracene derivative, yields determined by ^{1}H NMR analysis with 1,3,5-trimethoxybenzene as internal standard, isolated yields are shown in brackets. [a] Traces of dimerization product observed when 405 nm LED was employed. [b] 6 mL of DMSO was used. [c] Mixture of isomers.

be observed. We could only recover starting material despite the good Stern–Volmer quenching rates (for **12** k_{SV} = 4.1×10^9 $M^{-1}s^{-1}$, Figure S164) and the very low reduction potentials for these substrates (e.g., −1.16 V for phenazine).[44] It was noted that, when irradiated for 30 min, all reaction mixtures became red, while no color change was observed in the absence of light. Separated studies with selective irradiation of a 1:1 solution of PXX and **12** in DMSO under 405 nm showed the appearance of a red-shifted broad absorption band centered at 523 nm (Figure S169). Considering the broad nature of this electronic transition, we propose that a photoinduced electron donor–acceptor (EDA) complex is being formed under these conditions. As further selective irradiation at 535 nm did not trigger any transformations (and only starting materials were isolated), we hypothesize that an unreactive radical-ion pair complex [$PXX^{\bullet+}\cdot\mathbf{12}^{\bullet-}$] is formed, preventing the reaction from taking place. At last, attempts to reduce 2-amino-anthracene (**15**), anthracene-9-yl carboxylic acid (**16**), and phenanthrene (**17**) were unfruitful, with only starting material being recovered. In the case of phenanthrene (**17**), Stern–Volmer analysis revealed no PXX-centered fluorescence quenching (Figure S168), indicating that no electronic communication in the excited state occurs between the two species. Considering the high reduction potential of phenanthrene ($E_{1/2}^{M/M^{\bullet-}}$ = −2.49 V vs SCE),[45] it is apparent that ^{1}PXX* is not sufficiently reductive to undergo SET with this substrate. Stern–Volmer studies could not be performed in the case of 2-amino-anthracene due to spectral overlap with PXX (Figure S138).

Mechanistic investigations

To elucidate the mechanism of the PXX-triggered Birch-type photoreduction, we conducted another series of experiments with substrates **1**, **3**, and **5** employing [D_6]DMSO and [D_{15}]Et_3N as a sacrificial agent (deuterated DIPEA is not commercially available, Scheme S2). In [D_6]DMSO, non-deuterated reduced **1a** was obtained, strongly suggesting that the solvent is not implicated in any H-transfer reactions. Instead, when the reaction was performed in the presence of [D_{15}]Et_3N, deuterated derivative **D-1a** was obtained bearing a single D atom in position 9, advocating for an H-abstraction occurring at the α-position of the sacrificial amine. The same outcome was observed when both [D_{15}]Et_3N and [D_6]DMSO were used. 9-Methyl-anthracene (**3**) and 9-phenyl-anthracene (**5**) behaved similarly, yielding the corresponding monodeuterated products [D]-**3a** and [D]-**5a** featuring the D atom at the position 9, exclusively in the presence of [D_{15}]Et_3N. As one can expect, these studies suggest that the radical intermediate abstracting the H-atom is localized at the position 9, that is, the most substituted carbon atom. Taken all together, our experimental investigations and literature reports,[19] we can hypothesize that the photoreduction of anthracene is initiated by a SET process from ^{1}PXX* to anthracene (−1.97 V vs SCE)[46] leading to polar radicals $\mathbf{1}^{\bullet-}$ and $PXX^{\bullet+}$ intermediates (Scheme 3). Stern–Volmer investigations mirrored these considerations, showing that ^{1}PXX* is quenched by anthracene ($2.1–2.5\times10^9$ $M^{-1}s^{-1}$, Figur-

© 2023 The Authors. Chemistry - A European Journal published by Wiley-VCH GmbH



Scheme 3. Proposed reaction mechanism for the PXX-catalyzed photoreduction of anthracene derivatives.

es S159–S160) in DMSO either in the presence or absence of $HNTf_2$. Additional Stern–Volmer analyses showed that neither DIPEA nor DMSO itself either in the presence or absence of $HNTf_2$ (quenching measurements performed in CH_3CN) have a quenching effect on the ^{1}PXX* emission (Figures S156–S158). Considering the photoreduction studies performed with $[D_{15}]Et_3N$ and the lower yields obtained under these conditions, we hypothesize that $\mathbf{1}^{\bullet-}$ first undergoes H-abstraction from $DIPEA^{\bullet+}$ (or from DIPEA itself) to give anion $\mathbf{1}H^-$ and produce the iminium salt. The former undergoes protonation reaction with $HNTf_2$ to form 9,10-dihydroanthracene **1a**. The photocatalyst is restored from the oxidation of DIPEA to $DIPEA^{\bullet+}$ by $PXX^{\bullet+}$. As far as the parasitic cycloaddition reaction is concerned, this can occur only through direct excitation of the substrate. We excluded any PXX-mediated sensitization mechanism as no dimerization is observed for any of the substrates when PXX is selectively excited at 460 nm. As previously described by our group, the lack of phosphorescence and the photosensibility of PXX under laser excitation at 355 nm prevented us from collecting any information about the role of the dark triplet excited state ^{3}PXX*.[23] However, considering that the photoreductions are not performed under inert conditions, it is expected that the ^{3}PXX* is efficiently quenched by O_2. Thus, we hypothesize that, ^{3}PXX* has a marginal role in the reaction outcome under these experimental conditions.

PXX as heterogeneous photocatalyst

Having demonstrated the de-aromatization efficacy of PXX under homogeneous conditions we attempted the engineering of a heterogeneous system to be used both in batch and in continuous-flow reactors. Here, the objective was to develop a recyclable photocatalyst to enhance the sustainability of our synthetic approach. Specifically, we pursued the immobilization of PXX onto PDMS microparticles (PXX-PDMS). PDMS was chosen for being an attractive transparent, low-cost, inert, and thermally stable material, and its preparation easily scalable.[47–49] Firstly, PDMS beads of about 100 μm of diameter were synthesized by adapting a previously reported procedure (see Section 3 in the Supporting Information, for experimental details).[47] The beads presented an average diameter of 97.8 μm, with a polydispersity index of 0.22. We found it crucial to filter the PDMS beads using a pluriStrainer® 70 μm to remove satellite beads (20–30 μm), improving the polydispersity and avoiding the build-up of back-pressure in the final continuous-flow reactor (Figures 1 and S16). To graft PXX onto the PDMS beads, we designed and synthesized a PXX derivative bearing a (3-aminopropyl)triethoxy silane (APTES; **24**) moiety, enabling straightforward base-catalyzed condensation with the silanol groups onto the microparticles (Figure 1).[50]

To improve the solubility of the chromophore, molecule **24** was further equipped with a xylyl substituent (see Section 3 in the Supporting Information). A reference PXX-derivative bearing a xylyl moiety and *n*-propyl amide was also synthesized (**25**; see Section 3 in the Supporting Information) and its photophysical properties analyzed. As shown in Table 2, the spectral absorp-

© 2023 The Authors. Chemistry - A European Journal published by Wiley-VCH GmbH

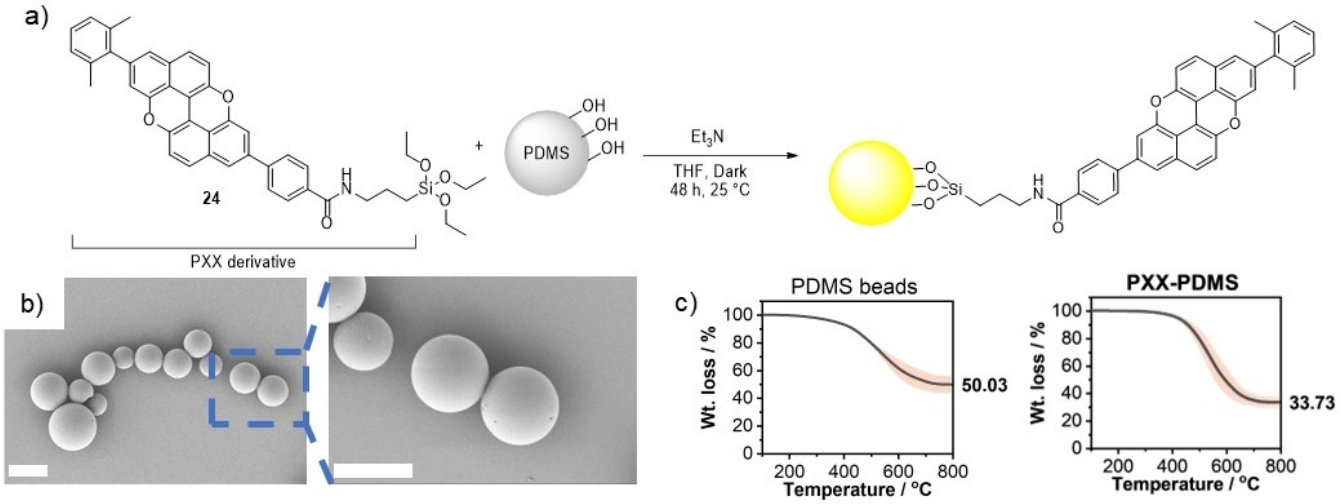


Figure 1. a) Schematic representation of the PXX-PDMS synthesis. b) SEM images of PXX-PDMS. Scale bars: 100 μm. c) Thermogravimetric analysis of PDMS beads and PXX-PDMS. Solid lines represent the average of three measurements, and pink shading represents the standard deviation of the measurements.

Table 2. Summary of photophysical and electrochemical properties of PXX, PXX derivative **25**, pristine PXX-PDMS, and PXX-PDMS after five catalytic cycles.

Sample	λ_{ex} [nm]	λ_{em} [nm]	Φ [%]	τ [ns]	$E^{ox}_{1/2}$ [V vs Fc/Fc$^+$]
PXX[a]	443	450	61[52]	6.8	0.32
25[a]	446	453	58	8.7	0.31
PXX-PDMS[b]	445	446	2	6.7	–
PXX-PDMS after 5 cycles[b]	445	447	2	6.0	–

[a] Measured in DMSO. [b] Measured in solid state.

tion and emission envelopes of PXX-amide derivative **25** matches that of unsubstituted PXX in solution. As the absorption maximum (λ_{max} = 446 nm) and oxidation potential ($E^{ox}_{1/2}$ = 0.31 V vs Fc/Fc$^+$) of PXX-amide conjugate **25** exhibits only a slight shift compared to PXX (λ_{max} = 443 nm, $E^{ox}_{1/2}$ = 0.32 V vs Fc/Fc$^+$), we conclude that both derivatives should exhibit similar photocatalytic properties.

Next, we proceeded with the grafting of photocatalyst **24** onto the PDMS-based solid support. The beads were dispersed in THF and stirred at room temperature in the presence of **24** and Et_3N for 2 days in the dark (Figure 1; see the Supporting Information for experimental details).[43,50] The functionalized beads were collected by filtration onto a pluriStrainer® 70 μm filter, and thoroughly washed with H_2O, Et_2O, and THF to remove impurities and the physiosorbed photocatalyst. Dialysis in THF was finally performed to ensure the removal of all remaining physiosorbed photocatalyst on the microparticles surface. This process was followed spectroscopically, and the dialysis cycles protracted until excitation and emission of the bulk dry PXX-PDMS resulted constant (Table 2; emission profile for pure hybrids in Figure S146). Dry PXX-PDMS was hence analyzed by thermogravimetric analysis (TGA; Figures 1 and S173) to determine the amount of grafted PXX, important to calculate the loading of beads in the photocatalyzed reduction.

Compared to the bare PDMS particles, PXX-PDMS displayed an additional weight loss of around 16% ascribable to a 0.3 μmol mg^{-1} loading of **24** (Figures 1 and S172–S173). To confirm that the photophysical properties of PXX remained unaltered upon grafting onto the PDMS beads, emission and excitation spectra, lifetime, and quantum yield of PXX-PDMS were recorded in the solid state (Table 2, Figure 2). The spectral envelope of PXX-PDMS is similar to that of **25** in solution, displaying pronounced vibronic substructures. As evidenced in Table 2, the excitation λ_{ex} and emission λ_{em} maxima exhibited only small (2–3 nm) shifts as well as similar lifetime values (8.7 and 6.7 ns for **25** and PXX-PDMS, respectively), indicating that the photophysical properties are only slightly affected by the PDMS-grafting. As expected, PXX-PDMS displays a considerably lower fluorescence quantum yield (2%) in the solid state when compared to that of free **25** in solution (61%). Fluorescence quenching is typically observed when a fluorophore is attached to solid particles. This can be ascribed to intermolecular energy transfer phenomena and inner filter effects when the material is aggregated in the solid state.[51] The photocatalytic activity and recyclability of PXX-PDMS were first evaluated in batch, by performing the heterogeneous reduction of 9-phenylanthracene (**5**) to derivative **5a**. Compared to the unsubstituted anthracene, substrate **5** is fully soluble under our reaction conditions (0.08 M in DMSO at RT).

Full solubility of starting material is crucial to develop a protocol for a continuous-flow reaction, avoiding the build-up of undesired backpressure. Moreover, aware of the instability of PDMS towards strong acids,[52] the use of $HNTf_2$ was avoided. 20 mg of supported catalyst was employed, resulting in an approximated catalyst loading of 6 μmol, in contrast to the 10 μmol of free PXX employed for the homogeneous photoreduction.

© 2023 The Authors. Chemistry - A European Journal published by Wiley-VCH GmbH

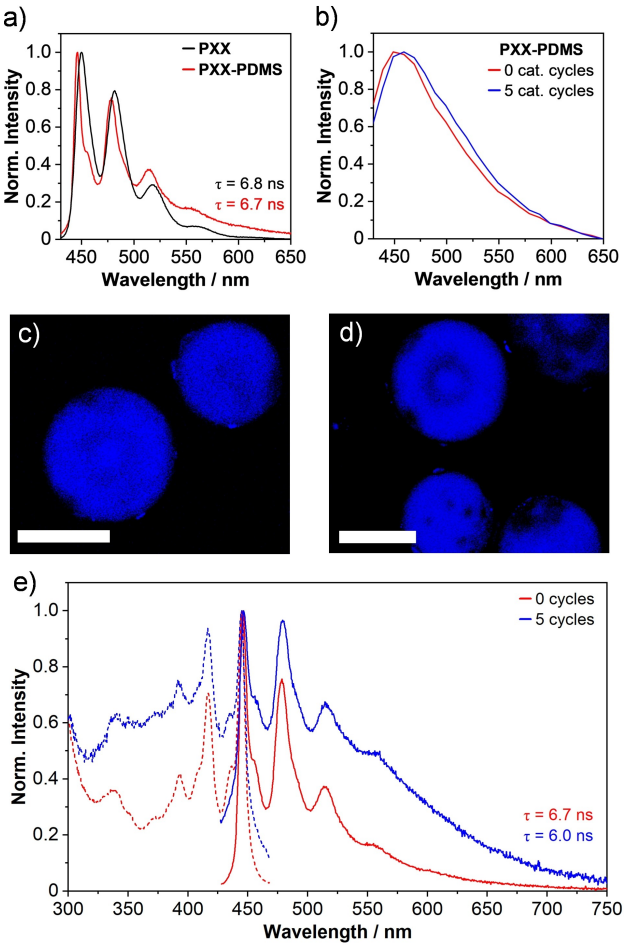
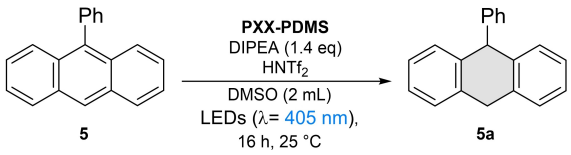


Figure 2. a) Emission spectra of PXX in solution and solid PXX-PDMS. b) Emission spectra obtained from the average of confocal images of pristine PXX-PDMS and PXX-PDMS after five catalytic cycles. Confocal images of c) pristine PXX-PDMS and d) PXX-PDMS after five catalytic cycles. λ_{ex} = 405 nm, scale bars: 100 μm. e) Emission (λ_{ex} = 417 nm, dashed line) and excitation (λ_{em} = 450 nm, solid line) spectra of pristine PXX-PDMS and PXX-PDMS after five catalytic cycles.

Table 3. Optimization of heterogeneous photocatalysis reaction conditions for **5a**.[a]



	Variation	Yield [%][b]
1	–	68
2[c]	2nd use same PXX-PDMS	68
3[c]	3rd use same PXX-PDMS	67
4[c]	4th use same PXX-PDMS	68
5[c]	5th use same PXX-PDMS	67
6	λ = 460 nm (instead of 405 nm)	54
7	20 mg of PDMS	–
8	Reaction performed in the dark	–
9	Reaction performed without DIPEA	–

[a] The reaction was performed using 0.5 mmol of **5**, and 20 mg of PXX-PDMS. [b] Yields determined by ^{1}H NMR analysis using 1,3,5-trimethoxybenzene as internal standard. [c] PXX-PDMS were filtered off the reaction mixture, extensively washed with DMSO and Et_2O, dried at RT, and used for the reaction.

After irradiation for 16 h (λ_{ex} = 405 nm), as reported in the optimized procedure, the heterogeneous photocatalyst afforded hydrogenated product **5a** in comparable yields (68%, Table 3) to those obtained under homogenous conditions (74%, Figure S71). As comparable yields to those obtained in the homogenous phase were obtained with lower catalyst loading (6 μmol for PDMS-PXX and 10 μmol of PXX), we conjectured that beads-immobilization reduces detrimental aggregation phenomena in solution when poorly soluble chromophores are used.[41] Control experiments confirmed that, when employing unfunctionalized PDMS microparticles, the photoreduction does not take place (Table 3, entry 7). Taken together, these results strongly suggest that the grafting on PDMS beads does not affect the photoreactivity of the *peri*-xanthenoxanthene core. After completion of the reaction, the supported catalyst could be easily recovered by filtration and recycled after washing with DMSO and Et_2O (to remove adsorbed unreacted components from the reaction mixture). The same batch of PXX-PDMS beads was then reused in the same reaction conditions up to five times. From the results reported in Table 3, it is clear that PXX-PDMS maintained the same catalytic activity throughout the five reaction cycles (i.e., average 68% yield). Supplementary control experiments were performed and confirmed that irradiation (λ_{ex} = 405 or 460 nm) and DIPEA are all necessary for the reaction to occur (Table 3, entries 7, 8). The excitation and emission spectra, lifetime, and quantum yield of the collected microparticles after the 5th cycle were also recorded and compared to those measured with the as-prepared beads (Figure 2, Table 2). A slight decrease (0.7 ns) in the fluorescence lifetime was observed after 5 photocatalytic cycles (such a difference is within the experimental error intrinsic to highly scattering samples).[54]

To further corroborate these results, confocal microscope imaging was also performed on the beads before and after five catalytic cycles. Visually, the beads retained their overall round shape and uniformity, indicating that no physical damage took place during the photochemical reaction or catalyst recovery. Spectroscopically, the broad emission profile also matches that of the as-prepared PXX-PDMS. These results further suggest that the supported catalyst is resilient under strong irradiation for prolonged times, making it a perfect candidate for use in a continuous-flow setting. To corroborate this hypothesis, we have integrated our heterogeneous photocatalyst in a home-designed microreactor-type apparatus and performed studies in continuous flow. Specifically, a suspension of PXX-PDMS (50 mg) in EtOH (2 mL) was introduced in a custom-made glass tube (i.d. = 0.15 mm), equipped with a glass frit to keep the supported photocatalyst in place during the continuous-flow reaction (Figures 3, S3, and S4). Optimization of the reaction

© 2023 The Authors. Chemistry - A European Journal published by Wiley-VCH GmbH

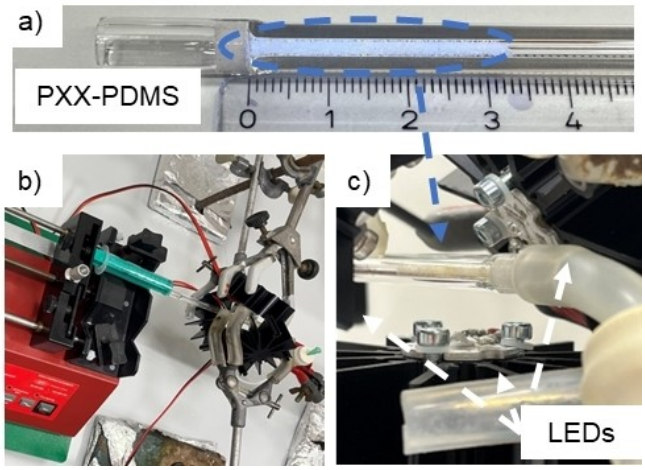


Figure 3. a) Glass tube filled with 50 mg of PXX-PDMS under UV light ($\lambda = 365$ nm); b) Packed bed continuous-flow set-up; c) Close-up of LEDs and filled glass tube.

conditions for the photoreduction of **5** was performed (Table S3).

The obtained yield is once again comparable to that obtained in the heterogeneous PXX-PDMS batch experiments (67–68%; Table 3). It is worth mentioning also that the same batch of the supported photocatalyst was kept in the reactor during the optimization process (up to 3 cycles), once more supporting the fact that our PXX-PDMS is very stable under the experimental conditions of the reaction and the possibility of recycling without reactivity loss. The flow rate was kept at 0.6 mL h^{-1}, molarity of starting material and number of LEDs used were optimized. The best yield (63%) was obtained with the following set-up (Figures 3 and S4): i) three LEDs, to ensure high power irradiation throughout the whole microreactor; ii) flow rate of 0.6 mL h^{-1}; iii) a 0.02 M concentration of **5** in DMSO.

Conclusions

In this paper, we have developed a novel photocatalyzed Birch-type chemoselective reduction of acenes by using *peri*-xanthenoxanthene as a reductive photocatalyst. We have shown that PXX can efficiently reduce anthracene derivatives under mild conditions, with high selectivity (yield = 24–75%). It has been hypothesized that the mechanism for the photoreduction involves a direct photoinduced electron transfer, hydrogen atom transfer, and a protonation step. When immobilized on PDMS beads, the PXX-based photocatalyst maintained its photoreductive properties and could be used as a supported catalyst in heterogenous photocatalysis, both in a batch and in a continuous-flow setting. However, our research also has some limitations and challenges that need to be addressed in future work. For example, we could not reduce some N-containing acenes due to the photoinduced formation of stable radical-ion pair complexes with PXX. Neither could we reduce phenanthrene due to its high reduction potential. Therefore, future research could explore the following aspects: i) designing new PXX derivatives or co-catalysts that can overcome the limitations of the current system and expand the substrate scope; ii) optimizing the reaction conditions and parameters to extend the chemical space of PXX-based photocatalysts; iii) applying the PXX-PDMS photocatalytic heterogenous system to other types of organic transformations that require reductive conditions.

Experimental Section

General information: instrumentation: Thin layer chromatography (TLC) was conducted on pre-coated aluminum sheets with 0.20 mm Machevery-Nagel Alugram SIL G/UV254 with fluorescent indicator UV254. Column chromatography was carried out using Merck Gerduran silica gel 60 (particle size 63–200 mm). Melting points (mp) were measured on a Gallenkamp apparatus in open capillary tubes and have not been corrected. Nuclear magnetic resonance: ^{1}H and ^{13}C NMR spectra were obtained with a Bruker Fourier 300 MHz spectrometer equipped with a dual (^{13}C, ^{1}H) probe, a Bruker Avance III HD 400 MHz NMR spectrometer equipped with a Broadband multinuclear (BBFO) SmartProbe™, a Bruker Avance III HD 500 MHz Spectrometer equipped with Broadband multinuclear (BBO) Prodigy CryoProbe or a Bruker AV III HDX 700 NMR spectrometer (Bruker BioSpin, Rheinstetten, Germany). The instrument is equipped with a quadruple (^{1}H, ^{13}C) inverse helium-cooled cryoprobe. Chemical shifts were reported in ppm according to tetramethylsilane using the solvent residual signal as an internal reference ($CDCl_3$: $\delta_H = 7.26$ ppm, $\delta_C = 77.16$ ppm). Coupling constants (J) were given in Hz. Resonance multiplicity was described as s (singlet), d (doublet), t (triplet), dd (doublet of doublets), dt (doublet of triplets), q (quartet), m (multiplet), and br (broad signal). Carbon spectra were acquired with a complete decoupling for the proton. Infrared spectra were recorded between 4000 and 400 cm^{-1} on a Bruker Alpha FTIR spectrometer in ATR mode. The absorption bands are reported in wavenumber (cm^{-1}). UV-vis Absorption spectroscopy was recorded on an Agilent Cary 5000 UV-Vis-NIR Spectrophotometer running in double beam mode with a matched pair of quartz absorbance cuvettes (1×1 cm). All absorption measurements were performed at 20 °C. Ultraviolet-visible emission spectroscopy: The photoluminescence (PL) excitation and emission spectra, absolute quantum yield, and decay curves were recorded on a FLS1000 photoluminescence spectrometer (Edinburgh Instruments, UK). The spectrometer was equipped with excitation and emission double grating Czerny-Turner monochromators, a photomultiplier (PMT) detector with extended near-infrared sensitivity (PMT980), thermoelectrically cooled to −20 °C with a fan-assisted Peltier element, and a high-speed PMT detector with a response width < 180 ps, operating at 0 °C. All samples were prepared in air-equilibrated DMSO (Abcr, Spectrophotometric grade, 99.9%) or Acetonitrile (Acros, Spectroscopy grade, 99+%). For steady-state measurements, the samples were excited using a 450 W ozone-free continuous Xenon arc lamp. Time-resolved measurements were performed by irradiating the samples with a picosecond-pulsed diode laser (EPL-405) and acquired using the high-speed PMT detector in time-correlated single photon counting (TCSPC) mode. The tail portion of the decay curves was fitted using the FAST software (Edinburgh Instruments, UK), following a single exponential model with y-offset (background-offset):

$$I(t) = A + B \cdot e^{\frac{-t}{\tau}} \quad (1)$$

© 2023 The Authors. Chemistry - A European Journal published by Wiley-VCH GmbH

where A is the y-offset, B is the pre-exponential factor, and τ is the lifetime. For decays close to the pulse width of the light source, the instrument response function (IRF) was measured using a Ludox® solution, adjusting the count rate with a computer-controlled neutral density filter wheel in order to match the sample emission. In these cases, the decay lifetime was obtained by performing a reconvolution fit, using the FAST software. Absolute quantum yields were measured using an integrating sphere (internal diameter 120 mm) fitted on the FLS1000 sample chamber. The samples and blank reference (solvent) were placed in a 1×1 cm fluorescence quartz cuvette and the calculations were done using the "direct excitation" method following the equation:

$$\Phi = \frac{E_B - E_A}{S_A - S_B} \# \quad (2)$$

where E_B and E_A correspond to the integrated fluorescence emission of the sample and blank reference (solvent), respectively. S_A and S_B refer to the integrated excitation scatter region of the reference and the sample, respectively. For measuring the scatter region, and avoid detector saturation, a neutral density filter (OD = 2) was placed between the integrating sphere exit and the detector in order to attenuate the signal. A fixed excitation bandwidth of 3 nm was used to ensure the determination of the sample absorption with high accuracy (step = 0.1 nm), while the emission bandwidth was chosen in order to obtain a strong sample emission signal (peak emission $> 10^4$ cps). A fluorescence quartz cuvette (1×1 cm) was used for all PL measurements in solution. For the measurement of powders, a demountable quartz cell (35×7×1 mm) was used, mounted in a front-face sample holder in a 90° geometry, tilted to 35°. Electrochemical analysis: Cyclic voltammetry experiments were performed at room temperature in a mixture of freshly distilled CH_2Cl_2, using an Autolab PGSTAT204 potentiostat (Metrohm, DE). A conventional three-electrode electrochemical cell connected to an argon source and an oil bubbler was used. Dry argon gas was bubbled through the sample solution for at least 15 min prior to each measurement and the headspace was continuously flushed throughout the experiment. A pre-bubbler filled with solvent was used in order to prevent evaporation. A glassy carbon disk (3 mm diameter) was used as a working electrode, Pt wire as auxiliary electrode, and an Ag/AgCl electrode as reference.

The glassy carbon working electrode was polished on a pad using diamond polish (1–15 μm) and washed with deionized water before each experiment; the Pt wire was flame-cleaned. Tetrabutylammonium hexafluorophosphate (Alfa Aesar, $TBAPF_6$) was twice recrystallized from absolute ethanol prior to use and it was added to the solution as a supporting electrolyte at a concentration of 0.1 M. Decamethylferrocene (Sigma Aldrich) or Ferrocene (Sigma Aldrich) was used as an internal reference. The formal redox potentials (half-wave potentials) were calculated using the formula:

$$E_{1/2} = \frac{E_{pa} + E_{pc}}{2} \# \quad (3)$$

where E_{pa} is the peak anodic potential and E_{pc} is the peak cathodic potential.

Mass spectrometry: i) High-resolution ESI mass spectra (HRMS) were performed on a Waters LCT HR TOF mass spectrometer in the positive or negative ion mode. ii) High-resolution ESI mass spectra (HRMS) were obtained on a maXis UHR ESI–Qq-TOF mass spectrometer in the positive or negative ion mode by direct infusion. The sum formulas of the detected ions were determined using Bruker Compass DataAnalysis 4.1 based on the mass accuracy ($\Delta m/z \leq 5$ ppm) and isotopic pattern matching (SmartFormula algorithm). HRLDMS spectra were acquired on a timsTOF fleX ESI/MALDI dual source – trapped ion mobility separation – Qq-TOF mass spectrometer in the positive ion mode. The sum formulas of the detected ions were determined using Bruker Compass DataAnalysis 5.3 based on the mass accuracy ($\Delta m/z \leq 5$ ppm) and isotopic pattern matching (SmartFormula algorithm). *Syringe pump* NE-4002X Programmable 2 Channel. *Confocal microscope* Zeiss LSM 710 laser-scanning confocal microscope equipped with an Elyra PS.1 system. For the spectral imaging, lambda stacks were acquired in the equatorial plane of the fluorescent microbeads using an EC Plan-NeoFluar 10X/0.30 objective. For excitation, a 405 nm diode laser was used, and the fluorescence emission was detected in the wavelength range of 424–654 nm. The pinhole diameter was set to 90 μm, and the spectral resolution was set to 10 nm step size. *SEM* images were recorded with a Zeiss Supra 55 VP instrument (Carl Zeiss, Germany) with an acceleration voltage of 5 kV. The sample was prepared by drop-casting the dispersion onto a Si substrate (1 cm^2), and subsequently, sputter coated with Au (Emitech K575X Peltier cooled) for 60 s at 60 mA prior to fixation on an Al support. Energy dispersive X-ray (EDS) spectroscopy mapping was performed at an acceleration voltage of 20 kV. *TGA* was performed with a TGA 550 instrument manufactured by TA instruments, under a N_2 flow of 60 mL·min^{-1} and with the following method: equilibration from room temperature to 100 °C, isothermal heating at 100 °C for 30 min, then ramp from 100 °C to 800 °C (heating rate of 10 °C min^{-1}).

General information: Materials and methods

Synthesis: 6-(2,6-Dimethylphenyl)naphthalen-2-ol (**18**) was prepared according to a literature procedure.[26] PXX was synthetized according to a modified literature procedure.[55] For synthesis of PXX-derivatives **24** and **25** see Scheme S1 and Section 3 of the Supporting Information. SYLGARD® 184 was purchased from *Dow*, pluriStrainer® filters were purchased from pluriSelect. Chemicals were purchased from BLDpharm, Sigma Aldrich, Acros Organics, TCI, Apollo Scientific, Fluorochem, and ABCR and were used without any further purification. Solvents were purchased from Sigma Aldrich, while deuterated solvents from Eurisotop. MeOH, $CHCl_3$, and acetone were purchased as reagent-grade and used without further purification. 0 °C temperature baths were prepared using ice/H_2O. Anhydrous conditions were achieved by drying Schlenk tubes or round-bottom flasks in an oven at 120 °C for at least 4 h, followed by evacuation under vacuum and purging with argon. Inert atmosphere was maintained using Argon-filled balloons equipped with a syringe and needle that was used to pierce the silicon stoppers used to close the flask's necks.

Experimental procedures

General procedure for homogeneous and heterogeneous photoreduction of acenes in solution: To a 20 mL Schlenk tube the substrate (0.5 mmol, 1 equiv), DIPEA (0.7 mmol, 1.4 equiv), $HNTf_2$ (10 mol%), PXX (2 mol%) or PDMS-PXX (20 mg), and DMSO were added under air. The reaction mixture was stirred and irradiated using 405 or 460 nm LED (if not differently stated LED output power used were respectively 17.7 and 15.7 mW cm^{-2}) at RT for 16 h. The reaction mixture was diluted with H_2O (10 mL), extracted with EtOAc (3×10 mL), washed with brine (30 mL), dried over $MgSO_4$, filtered and the solvent removed under reduced pressure. The crude was purified by flash chromatography (on SiO_2) eluting with heptane.

*9,10-Dihydroanthracene (**1a**)*: Synthesized according to the general procedure using anthracene (89 mg), DIPEA (91 mg), $HNTf_2$ (14 mg), PXX (0.3 mg), and DMSO (2 mL). The crude was purified by flash chromatography eluting with heptane (100%), to give **1a** as a white solid (62 mg, 0.34 mmol, 71% yield). ^{1}H NMR (400 MHz,

© 2023 The Authors. Chemistry - A European Journal published by Wiley-VCH GmbH

$CDCl_3$): $\delta = 7.33–7.28$ (m, 4H), 7.24–7.18 (m, 4H), 3.96 (s, 4H). ^{13}C NMR (101 MHz, $CDCl_3$): $\delta = 136.67$, 127.37, 126.07, 36.14. HRMS (EI) *m/z* calcd. for $[C_{14}H_{12}]^+$: 180.0939 $[M]^+$; found: 180.0928. Spectroscopic characterization in accordance with literature.[19]

*5,12-Dihydrotetracene (**2a**)*: Synthesized according to the general procedure using tetracene (114 mg), DIPEA (91 mg), $HNTf_2$ (14 mg), PXX (0.3 mg) and DMSO (6 mL). The crude was purified by flash chromatography eluting with heptane (100%), to give **2a** as a white solid (69 mg, 0.34 mmol, 60% yield). ^1H NMR (400 MHz, $CDCl_3$): $\delta = 7.81–7.77$ (m, 2H), 7.76 (s, 2H), 7.45–7.39 (m, 2H), 7.37–7.31 (m, 2H), 7.24–7.18 (m, 2H), 4.10 (s, 4H). ^{13}C NMR (101 MHz, $CDCl_3$): $\delta = 137.08$, 135.70, 132.35, 127.22, 127.19, 126.24, 125.27, 125.15, 36.81. HRMS (EI) *m/z* calcd. for $[C_{18}H_{14}]^+$: 229.1096 $[M]^+$; found: 229.1005. Spectroscopic characterization in accordance with literature.[56]

*9-Methyl-9,10-dihydroanthracene (**3a**)*: Synthesized according to the general procedure using 9-methyl-anthracene (96 mg), DIPEA (91 mg), $HNTf_2$ (14 mg), PXX (0.3 mg) and DMSO (2 mL). The crude was purified by flash chromatography eluting with heptane (100%), to give **3a** as a white solid (42 mg, 0.22 mmol, 43% yield). ^1H NMR (400 MHz, $CDCl_3$): $\delta = 7.22–7.14$ (m, 4H), 7.16–7.07 (m, 4H), 4.04 (d, $J = 18.2$ Hz, 1H), 3.96 (q, $J = 7.2$ Hz, 1H), 3.80 (d, $J = 18.2$ Hz, 1H), 1.35 (d, $J = 7.2$ Hz, 3H). ^{13}C NMR (101 MHz, $CDCl_3$): $\delta = 141.73$, 135.76, 127.65, 126.85, 126.34, 125.92, 41.07, 35.10, 23.48. HRMS (EI) *m/z* calcd. for $[C_{15}H_{14}]^+$: 194.1096 $[M]^+$; found: 194.0772. Spectroscopic characterization in accordance with literature.[19]

*9,10-Dimethyl-9,10-dihydroanthracene (mixture of 2 isomers) (**4a**)*: Synthesized according to the general procedure using 9,10-dimethylanthracene (104 mg), DIPEA (91 mg), $HNTf_2$ (14 mg), PXX (0.3 mg) and DMSO (2 mL). The crude was purified by flash chromatography eluting with heptane (100%), to give **4a** (as mixture of isomers in 1:0.55 *trans:cis* ratio) as a white solid (72 mg, 0.36 mmol, 72% yield). ^1H NMR (400 MHz, $CDCl_3$): $\delta = 7.33–7.28$ (m, 2.4H), 7.24–7.20 (m, 4.1H), 7.19–7.13 (m, 5.9H), 4.06–3.95 (m, 3.2H), 1.56 (d, $J = 7.1$ Hz, 3.3H), 1.49 (d, $J = 7.4$ Hz, 6H). ^{13}C NMR (101 MHz, $CDCl_3$): $\delta = 141.26$, 140.43, 127.81, 126.19, 126.13, 125.75, 39.98, 38.44, 28.51, 18.77. HRMS (ESI) *m/z* calcd. for $[C_{16}H_{16}]^+$: 208.1252 $[M]^+$; found: 208.1200. Spectroscopic characterization in accordance with literature.[57]

*9-Phenyl-9,10-dihydroanthracene (**5a**)*: Synthesized according to the general procedure using 9-phenyl-anthracene (127 mg), DIPEA (91 mg), $HNTf_2$ (14 mg), PXX (0.3 mg), and DMSO (2 mL). The crude was purified by flash chromatography eluting with heptane (100%), to give **5a** as a white solid (59 mg, 0.34 mmol, 60% yield). ^1H NMR (400 MHz, $CDCl_3$): $\delta = 7.29–7.17$ (m, 4H), 7.17–7.10 (m, 6H), 7.07–7.03 (m, 1H), 7.00–6.98 (m, 2H), 5.18 (s, 1H), 3.94 (d, $J = 18.2$ Hz, 1H), 3.82 (d, $J = 18.2$ Hz, 1H). ^{13}C NMR (101 MHz, $CDCl_3$): $\delta = 143.55$, 139.47, 136.41, 128.42, 128.41, 128.03, 127.75, 126.39, 126.36, 126.19, 51.42, 35.65. HRMS (EI) *m/z* calcd. for $[C_{20}H_{16}]^+$: 256.1252 $[M]^+$; found: 256.1245. Spectroscopic characterization in accordance with literature.[19]

*9,10-Diphenyl-9,10-dihydroanthracene (mixture of 2 isomers) (**6a**)*: Synthesized according to the general procedure using 9,10-diphenylanthracene (165 mg), DIPEA (91 mg), $HNTf_2$ (14 mg), PXX (0.3 mg), and DMSO (2 mL). The crude was purified by flash chromatography eluting with heptane (100%), to give **6a** (as a mixture of isomers in 1:0.1 *trans:cis* ratio) as white solid (83 mg, 0.25 mmol, 50% yield). ^1H NMR (400 MHz, $CDCl_3$): $\delta = 7.19–6.98$ (m, 20.5H), 5.25 (s, 2H), 5.17 (s, 0.3H). ^{13}C NMR (101 MHz, $CDCl_3$): $\delta =$ 144.38, 138.44, 131.34, 129.24, 129.22, 128.58, 128.43, 128.15, 126.98, 126.47, 126.13, 125.00, 49.94. HRMS (EI) *m/z* calcd. for $[C_{26}H_{20}]^+$: 332.1560 $[M]^+$; found: 332.1560. Spectroscopic characterization in accordance with literature.[58]

*Methyl 9,10-dihydroanthracene-9-carboxylate (**7a**)*: Synthesized according to the general procedure using methyl anthracene-9-carboxylate (119 mg), DIPEA (91 mg), $HNTf_2$ (14 mg), PXX (0.3 mg), and DMSO (2 mL). The crude was purified by flash chromatography eluting with heptane/ethyl acetate (80:20, *v/v*), to give **7a** as a white solid (33 mg, 0.14 mmol, 28% yield).^1H NMR (400 MHz, $CDCl_3$): $\delta = 7.33–7.31$ (m, 2H), 7.28–7.26 (m, 2H), 7.23–7.20 (m, 2H), 7.19–7.15 (m, 2H), 4.93 (s, 1H), 4.27–4.23 (d, $J = 18.2$ Hz, 1H), 3.85–3.81 (d, $J = 18.2$ Hz, 1H), 3.51 (s, 3H). ^{13}C NMR (101 MHz, $CDCl_3$): $\delta = 161.65$, 136.71, 128.27, 128.05, 127.51, 126.39, 126.25, 55.34, 52.87, 52.38. HRMS (EI) *m/z* calcd. for $[C_{16}H_{14}O_2]^+$: 238.0994 $[M]^+$; found: 238.0958. Spectroscopic characterization in accordance with literature.[6]

***N*-(9,10-Dihydroanthracen-2-yl)acetamide (8a)**: Synthesized according to the general procedure by using *N*-(anthracen-2-yl)acetamide (118 mg), DIPEA (91 mg), $HNTf_2$ (14 mg), PXX (0.3 mg), and DMSO (2 mL). The crude was purified by flash chromatography eluting with heptane/ethyl acetate (75:25, *v/v*), to give **8a** as a white solid (28 mg, 0.12 mmol, 24% yield).^1H NMR (400 MHz, $CDCl_3$): $\delta = 7.46$ (s, 1H), 7.30 (br s, 1H), 7.21–7.17 (m, 2H), 7.15–7.14 (m, 2H), 7.12–7.10 (m, 2H), 3.82 (s, 4H), 2.09 (s, 3H). ^{13}C NMR (101 MHz, $CDCl_3$): $\delta = 168.29$, 137.47, 135.54, 136.31, 135.90, 134.25, 133.85, 129.23, 127.76, 127.43, 127.37, 136.13, 119.18, 117.82, 36.21, 35.55. HRMS (EI) *m/z* calcd. for $[C_{16}H_{15}NO]^+$: 237.1154 $[M]^+$; found: 237.1229. mp 53–54 °C. IR (ATR): ν (cm^{-1}) = 734, 762, 841, 924, 1009, 1131, 1411, 1460, 1474, 1489, 1500, 1751, 2821, 2984, 3031, 3066, 3415.

PDMS beads: Polydimethylsiloxane (PDMS) beads were obtained by adapting a co-flow microfluidic approach (Figure S15) previously reported.[46] Discontinuous phase was prepared solubilizing 2.75 g (component A/component B, 10/1) of the SYLGARD® 184 in 55 g of CH_2Cl_2 (5 $\%_{w/w}$). PVA 3 $\%_{w/w}$ aqueous solution was used as the collection (300 mL) and continuous phases. Both continuous and discontinuous phases were loaded into two different 20 mL glass syringes. The flow rate of the continuous phase was set to 900 μL min^{-1} while the discontinuous phase flow rate was set to 150 μL min^{-1} with the use of syringe pumps. Flows were optimized to obtain beads with a diameter of about 100 μm. The PDMS droplets flowed along the capillary into a tall beaker (500 mL) containing 300 mL of gently stirred collection phase. To allow slow solvent evaporation, the solution was gently stirred overnight. PDMS beads curing was induced by heating the beads to 40 °C for 3 h, followed by heating to 80 °C for 3 h. The suspension was filtered using a pluriStrainer® 70 μm and dispersed in 80 °C H_2O. The suspension was then centrifugated three times at 5000 rpm for 5 min. Between each centrifugation cycle, the supernatant was carefully removed and replaced with 80 °C H_2O to remove traces of PVA derived from the continuous and collecting phases. The effectiveness of PVA removal was monitored by TGA (see Section 8 in the Supporting Information). Decanted PDMS beads were taken in Et_2O and after evaporation of the solvent at RT, dry PDMS beads were obtained (Figure S16).

PXX-PDMS: PDMS beads (50 mg) and 3 drops of Et_3N were added to a solution of **24** (0.039 mmol)* in stabilized THF (5 mL), and the suspension was stirred for 48 h at RT in the dark. After the reaction time, the beads were filtered off with a pluriStrainer® filter with a pore size of 70 μm. The collected beads were washed extensively with H_2O, Et_2O, and THF to remove all the impurities and the aspecifically attached photocatalyst. PXX-PDMS purification was performed by dialysis for up to 7 days in THF (1.5 L), replacing the buffer solution with fresh THF every 24 h. Effective purification of beads was determined by spectroscopic analysis (excitation, emission, and lifetime). After complete dialysis, the beads were collected, washed with THF, and dried at RT. *Estimated value considering a quantitative yield for the synthesis of compound **24**.

© 2023 The Authors. Chemistry - A European Journal published by Wiley-VCH GmbH

General procedure for continuous-flow photoreduction: A suspension of PXX-PDMS (50 mg) in ethanol was taken with a 2 mL syringe. The syringe was connected to the input of the glass reactor and a gentle pressure was applied. Ethanol passed all the way through the glass reactor and the PXX-PDMS stayed in the reactor blocked from the frit filter. The process was repeated with more ethanol until all the PXX-PDMS were allocated into the glass reactor. Finally, the beads were dried with an Ar flow. The reaction mixture was filtered before and after being taken up with a 10 mL syringe. The syringe was placed on a syringe pump. The tip of the syringe was connected to the inlet of the filled glass reactor. The outlet of the glass reactor was connected to the collection flask through a PVC tube. The reactor apparatus was wrapped in aluminium foil, except for the area where the supported photocatalyst is allocated and exposed to irradiation, 1 or 3 LEDs were used as shown in section 1.2. The reaction was started by turning on the LEDs and syringe pump. After the set reaction time, the reactor was flushed with additional DMSO (2 mL) in order to recover all the reaction mixture.

Supporting Information

The authors have cited additional references within the Supporting Information.[59,60]

Acknowledgements

D. B. gratefully acknowledges the EU through the MSCA-ITN-ETN (project: PHOTOTRAIN, no. 722591), MSCA-RISE (project: INFUSION, no. 734834; VIT, no. 101008237), and the University of Vienna for generous financial support. We thank the NMR and Mass service centers at the Faculty of Chemistry of the University of Vienna for the spectroscopic and spectrometric characterization of the products prepared in this work. In particular, we thank Ass. Prof. H. Khalig for the constant support in the NMR characterization and interpretation of the data. We thank The Core Facility Multimodal Imaging of the Faculty of Chemistry for the confocal microscope pictures. We acknowledge Raimund Schubert for manufacturing the custom glass microreactor.

Conflict of Interests

The authors declare no conflict of interest.

Data Availability Statement

The data that support the findings of this study are available from the corresponding author upon reasonable request.

Keywords: acenes · Birch reduction · photocatalysis · PXX

[1] A. J. Birch, *J. Chem. Soc.* **1942**, *66*, 430–436.
[2] A. J. Birch, *J. Chem. Soc.* **1945**, *67*, 809–813.
[3] A. J. Birch, *J. Chem. Soc.* **1946**, *68*, 593–597.
[4] B. J. Mortensen, J. Heinze, *Angew. Chem. Int. Ed. Engl.* **1984**, *23*, 84–85.
[5] B. K. Peters, K. X. Rodriguez, S. H. Reisberg, S. B. Beil, D. P. Hickey, Y. Kawamata, M. Collins, J. Starr, L. Chen, S. Udyavara, K. Klunder, T. J. Gorey, S. L. Anderson, M. Neurock, S. D. Minteer, P. S. Baran, *Science* **2019**, *363*, 838–845.
[6] M. Szostak, M. Spain, D. J. Procter, *J. Org. Chem.* **2014**, *79*, 2522–2537.
[7] P. Lei, Y. Ding, X. Zhang, A. Adijiang, H. Li, Y. Ling, J. An, *Org. Lett.* **2018**, *20*, 3439–3442.
[8] P. Nandi, J. L. Dye, J. E. Jackson, *J. Org. Chem.* **2009**, *74*, 5790–5792.
[9] J. Burrows, S. Kamo, K. Koide, *Science* **2021**, *374*, 741–746.
[10] Z. Shi, N. Li, H. K. Lu, X. Chen, H. Zheng, Y. Yuan, K. Y. Ye, *Curr. Opin. Electrochem.* **2021**, *28*, 100713.
[11] D. S. Lee, A. Love, Z. Mansouri, T. H. Waldron Clarke, D. C. Harrowven, R. Jefferson-Loveday, S. J. Pickering, M. Poliakoff, M. W. George, *Org. Process Res. Dev.* **2022**, *26*, 2674–2684.
[12] Y. Gao, K. Kubota, H. Ito, *Angew. Chem. Int. Ed.* **2023**, *62*, e202217723.
[13] N. Davison, J. A. Quirk, F. Tuna, D. Collison, C. L. McMullin, H. Michaels, G. H. Morritt, P. G. Waddell, J. A. Gould, M. Freitag, J. A. Dawson, E. Lu, *Chem.* **2023**, *9*, 576–591.
[14] D. Kim, T. S. Teets, *Chem. Phys. Rev.* **2022**, *3*, 021302.
[15] M. H. Shaw, J. Twilton, D. W. C. MacMillan, *J. Org. Chem.* **2016**, *81*, 6898–6926.
[16] H. Li, X. Tang, J. H. Pang, X. Wu, E. K. L. Yeow, J. Wu, S. Chiba, *J. Am. Chem. Soc.* **2021**, *143*, 481–487.
[17] E. H. Discekici, N. J. Treat, S. O. Poelma, K. M. Mattson, Z. M. Hudson, Y. Luo, C. J. Hawker, J. R. De Alaniz, *Chem. Commun.* **2015**, *51*, 11705–11708.
[18] I. Ghosh, T. Ghosh, J. I. Bardagi, B. König, *Science* **2014**, *346*, 725–728.
[19] A. Chatterjee, B. König, *Angew. Chem. Int. Ed.* **2019**, *131*, 14427–14432.
[20] J. P. Cole, D. F. Chen, M. Kudisch, R. M. Pearson, C. H. Lim, G. M. Miyake, *J. Am. Chem. Soc.* **2020**, *142*, 13573–13581.
[21] T. Yuan, L. Sun, Z. Wu, R. Wang, X. Cai, W. Lin, M. Zheng, X. Wang, *Nat. Catal.* **2022**, *5*, 1157–1168.
[22] E. Y. K. Tan, A. S. Mat Lani, W. Sow, Y. Liu, H. Li, S. Chiba, *ChemRxiv.* preprint, **2023**, 10.26434/chemrxiv-2023-kccqn.
[23] A. Sciutto, A. Fermi, A. Folli, T. Battisti, J. M. Beames, D. M. Murphy, D. Bonifazi, *Chem. Eur. J.* **2018**, *24*, 4382–4389.
[24] C. Pezzetta, A. Folli, O. Matuszewska, D. Murphy, R. W. M. Davidson, D. Bonifazi, *Adv. Synth. Catal.* **2021**, *363*, 1–15.
[25] T. Miletić, A. Fermi, I. Orfanos, A. Avramopoulos, F. De Leo, N. Demitri, G. Bergamini, P. Ceroni, M. G. Papadopoulos, S. Couris, D. Bonifazi, *Chem. Eur. J.* **2017**, *23*, 2363–2378.
[26] D. Stassen, N. Demitri, D. Bonifazi, *Angew. Chem. Int. Ed.* **2016**, *55*, 5947–5951.
[27] A. Berezin, N. Biot, T. Battisti, D. Bonifazi, *Angew. Chem. Int. Ed.* **2018**, *57*, 8942–8946.
[28] A. L. Trifonov, L. I. Panferova, V. V. Levin, V. A. Kokorekin, A. D. Dilman, *Org. Lett.* **2020**, *22*, 2409–2413.
[29] Q. Ma, J. Song, X. Zhang, Y. Jiang, L. Ji, S. Liao, *Nat. Commun.* **2021**, *12*, 1–8.
[30] P. Wang, H. Zhang, M. Zhao, S. Ji, L. Lin, N. Yang, X. Nie, J. Song, S. Liao, *Angew. Chem. Int. Ed.* **2022**, *61*, 1–9.
[31] H. Zhang, N. Yang, J. Li, P. Wang, S. Li, L. Xie, S. Liao, *Org. Lett.* **2022**, *24*, 8170–8175.
[32] L. Lin, P. Wang, T. Dong, G. C. Tsui, S. Liao, *Org. Lett.* **2023**, *25*, 1088–1093.
[33] P. Wang, S. J. Li, H. Zhang, N. Yang, S. Liao, *Synlett.* **2023**, *34*, 471–476.
[34] B. Castanheira, F. de Jesus Trindade, L. dos Santos Andrade, I. L. Nantes, M. J. Politi, E. R. Triboni, S. Brochsztain, *J. Photochem. Photobiol. A* **2017**, *332*, 316–325.
[35] D. González-Muñoz, A. Gómez-Avilés, C. B. Molina, J. Bedia, C. Belver, J. Alemán, S. Cabrera, *J. Mater. Sci. Technol.* **2022**, *103*, 134–143.
[36] H. S. Zakria, M. H. D. Othman, R. Kamaludin, S. H. Sheikh Abdul Kadir, T. A. Kurniawan, A. Jilani, *RSC Adv.* **2021**, *11*, 6985–7014.
[37] T. H. Rehm, *Chem. Eur. J.* **2020**, *26*, 16952–16974.
[38] C. Sambiagio, T. Noël, *Trends Chem.* **2020**, *2*, 92–106.
[39] D. Cambié, C. Bottecchia, N. J. W. Straathof, V. Hessel, T. Noël, *Chem. Rev.* **2016**, *116*, 10276–10341.
[40] C. Yang, R. Li, K. A. I. Zhang, W. Lin, K. Landfester, X. Wang, *Nat. Commun.* **2020**, *11*, 1–8.
[41] A. Hennig, S. Hatami, M. Spieles, U. Resch-Genger, *Photochem. Photobiol. Sci.* **2013**, *12*, 729.
[42] H. Bouas-Laurent, A. Castellan, J. P. Desvergne, R. Lapouyade, *Chem. Soc. Rev.* **2000**, *29*, 43–55.

© 2023 The Authors. Chemistry - A European Journal published by Wiley-VCH GmbH

[43] H. Bouas-Laurent, J.-P. Desvergne, A. Castellan, R. Lapouyade, *Chem. Soc. Rev.* **2001**, *30*, 248–263.
[44] C. De La Cruz, A. Molina, N. Patil, E. Ventosa, R. Marcilla, A. Mavrandonakis, *Sustain. Energy Fuels* **2020**, *4*, 5513–5521.
[45] G. J. Hoijtink, *Recl. Trav. Chim. Pays-Bas* **1958**, *77*, 555–558.
[46] V. D. Parker, *J. Am. Chem. Soc.* **1976**, *98*, 98–103.
[47] S. W. Choi, I. W. Cheong, J. H. Kim, Y. Xia, *Small* **2009**, *5*, 454–459.
[48] D. R. Jun, S. K. Moon, S. W. Choi, *Colloids Surf. B.* **2014**, *121*, 395–399.
[49] S. C. Lesher-Pérez, G. A. Kim, C. H. Kuo, B. M. Leung, S. Mong, T. Kojima, C. Moraes, M. D. Thouless, G. D. Luker, S. Takayama, *Biomater. Sci.* **2017**, *5*, 2106–2113.
[50] L. Tang, N. Y. Lee, *Lab Chip.* **2010**, *10*, 1274.
[51] P. P. Pompa, G. Ciccarella, J. Spadavecchia, R. Cingolani, G. Vasapollo, R. Rinaldi, *J. Photochem. Photobiol. A* **2004**, *163*, 113–120.
[52] A. Mata, A. J. Fleischman, S. Roy, *Biomed. Microdevices.* **2005**, *7*, 281–293.
[53] C. Valentini, D. Gowland, C. G. Bezzu, D. Romito, N. Demitri, N. Bonini, D. Bonifazi, *Chem. Sci.* **2022**, *13*, 6335–6347.
[54] V. Y. Soloviev, K. B. Tahir, J. McGinty, D. S. Elson, M. A. A. Neil, P. M. W. French, S. R. Arridge, *Appl. Opt.* **2007**, *46*, 7384.
[55] T. Kamei, M. Uryu, T. Shimada, *Org. Lett.* **2017**, *19*, 2714–2717.
[56] R. Dorel, P. R. McGonigal, A. M. Echavarren, *Angew. Chem. Int. Ed.* **2016**, *55*, 11120–11123.
[57] P. Stegner, C. Färber, U. Zenneck, C. Knüpfer, J. Eyselein, M. Wiesinger, S. Harder, *Angew. Chem. Int. Ed.* **2021**, *60*, 4252–4258.
[58] B. Il Yoo, Y. J. Kim, Y. You, J. W. Yang, S. W. Kim, *J. Org. Chem.* **2018**, *83*, 13847–13853.
[59] E. Le Saux, M. Zanini, P. Melchiorre, *J. Am. Chem. Soc.* **2022**, *144*, 1113–1118.
[60] M. E. Due-Hansen, S. K. Pandey, E. Christiansen, R. Andersen, S. V. F. Hansen, T. Ulven, *Org. Biomol. Chem.* **2016**, *14*, 430–433.

Manuscript received: July 4, 2023
Accepted manuscript online: August 18, 2023
Version of record online: October 4, 2023

© 2023 The Authors. Chemistry - A European Journal published by Wiley-VCH GmbH